Anisotropic scattering and travel time delay analysis in Kilauea volcano, Hawaii, earthquake coda waves

Jean-Luc Got[1]

Laboratoire d'Instrumentation Géophysique, Université de Savoie, Le Bourget-du-Lac, France

Olivier Coutant

Laboratoire de Géophysique Interne et Tectonophysique, CNRS, Université Joseph Fourier, Grenoble, France

Abstract. We study the S wave coda of microearthquake multiplets (earthquakes showing similar seismograms) recorded on the Kilauea volcano, and we analyze the direction of emission for wavelets composing the coda. Our data set consists of 71 small magnitude, well-relocated, clustered events that occurred in an area of about 1 km^2 in the southern flank of Kilauea, recorded at hypocentral distances of 10 to 20 km. For each station, we apply a cross-spectral moving-window technique to each pair of multiplet records to estimate the travel time delays due to source location offsets. These delays are computed for consecutive windows, starting at the P wave arrival time and ending at 4 times the S wave travel time. They are next used to estimate the slowness vector for each window along the seismograms. Our analysis shows (1) that scattered waves are emitted anisotropically along some preferred directions as late as 4 times the S wave travel time, and (2) that for some stations, the azimuthal plane rotates during the seismogram with a clear travel time delay signature. Our analysis shows that travel time delay variation in the coda can be purely due to geometrical propagation effects. This conclusion is of special interest when trying to use travel time delays to infer temporal changes in the crust. Our results do not support a coda diffracted isotropically in the crust, in the magnitude range and at the hypocentral distances we investigated.

Introduction

Following the general definition, coda waves are defined as the wave trains following the arrival of the direct wave fronts in seismograms. There are, of course, coda waves after each major phase arrival in seismograms, ranging from teleseismic to local propagation, at any wavelength (e.g., L_g coda [*Dainty and Toksöz*, 1990]). Coda of local earthquakes, however, has generated a lot of interest since the pioneer work of *Aki and Chouet* [1975] (see *Herraiz and Espinoza* [1987], and *Sato* [1991], for reviews). *Aki and Chouet*'s [1975] single backscattering model has been the first widely used model for the late coda of local earthquakes. It notably provides a practical tool to estimate S wave crustal attenuation and monitor its temporal variations. In this model, a late coda is defined as the part of the coda for which the decay is independent of the recording station. This part of the coda is therefore expected to be composed of wavelets which are randomly scattered in the crust. This late coda was empirically found by *Rautian and Khalturin* [1978] to be later than approximately twice the S wave travel time ($2t_s$), the part between t_s and $2t_s$ being called early coda; $2t_s$ has been thereafter recognized by most authors as the beginning of the late, crustal coda.

More recently, *Spudich and Miller* [1990] decomposed clearly the coda of local earthquakes into two separate Green's functions.

The coda is therefore seen as the convolution of a crustal or lithospheric response by a more or less local site response. As long as linear elasticity holds, this site response can be studied with small magnitude earthquakes to quantify amplifications, valley reverberation, and other site effects [*Phillips and Aki*, 1986; *Mayeda et al.*, 1991; *Spudich and Iida*, 1993]. On the other hand, the lithospheric response can be used as a prospecting tool to image the crust [*James et al.*, 1987] or, assuming that it is governed by the statistical properties of the medium, to study attenuation [*Aki and Chouet*, 1975; *Herraiz and Espinosa*, 1987; *Mayeda et al.*, 1992] or the statistics of the medium itself [*Sato*, 1991; *Hoshiba*, 1995]. Depending on our field of interest (site or lithospheric response), questions remain concerning the part of the coda that we can or must use: where does the coda transition between a local response and the diffraction in the lithosphere occur? Which part can be studied deterministically, and which part can, or must, be studied statistically?

To study these questions the coda wavefield of local earthquakes has been analyzed, on the one hand, close to the receivers using arrays of stations with both surface and borehole instruments [e.g., *Al-Shukri et al.*, 1995]. These studies point out the importance of very local and superficial slow layers in coda generation at high frequencies. They cannot however discriminate between a local or crustal coda. *Spudich and Bostwick* [1987], on the other hand, analyzed the wave field close to the source area using an array of sources instead. Their work and a similar study performed by *Scherbaum et al.* [1991] show that a separation occurs in the coda generation process around $2t_s$ between local coda before and crustal coda after. However, *Mayeda et al.* [1991] observed that coda decay of microearthquakes recorded at Long Valley could become common to the stations after a lapse time much greater than $2t_s$. More recently, *Xie et al.* [1996], using

Spudich and Bostwick's [1987] method with microearthquake clusters of the New Madrid seismic zone, did not find any clear transition from local to crustal scattering around $2t_s$.

In this work we follow *Spudich and Bostwick's* [1987] original idea based on reciprocity to apply array methods to arrays of sources, and we use a remarkably dense cluster of similar earthquakes to examine the coda wave field near the source area. We focus our analysis on travel time differences due to source offsets, computed using the cross-spectral method, rather than on the *F-K* slowness analysis used previously. Using a travel time delay analysis, we address the following questions: which part of the travel time difference is really due to the different source locations, and which part could be due to travel path perturbations between the occurrences of the different events constituting our multiplet? These questions have interesting consequences when using coda travel time difference as a signature of medium perturbation, as has been proposed by *Poupinet et al.* [1984] and *Ratdomopurbo and Poupinet* [1995]. Once the origin of these travel time differences is clear, we analyze the slowness directions for plane waves leaving the

source region and propagating in a highly heterogeneous medium such as Kilauea volcano.

Data

The data set consists of microearthquakes recorded between 1979 and 1983 by the Hawaiian Volcano Observatory (HVO) seismic network, which at that time was operating 50 telemetered stations distributed throughout the island of Hawaii. The events used in this study (Figure 1a) have been selected from a 250-event set constituting the large multiplet relocated in the south flank of Kilauea by *Got et al.* [1994]. Major geological features of Kilauea volcano are Kilauea caldera, from which radiate two large rift zones delimiting the south flank. The south flank of Kilauea volcano slides southward along a near-horizontal slip plane, whose depth (8 to 9 km) coincides with that of the top of the sediment layer surrounding the oceanic crust. Two major normal fault systems (Koae fault system and Hilina fault system) run through the south flank of Kilauea volcano. Hilina fault system is responsible for the huge (up to 500 m high) fault scarps
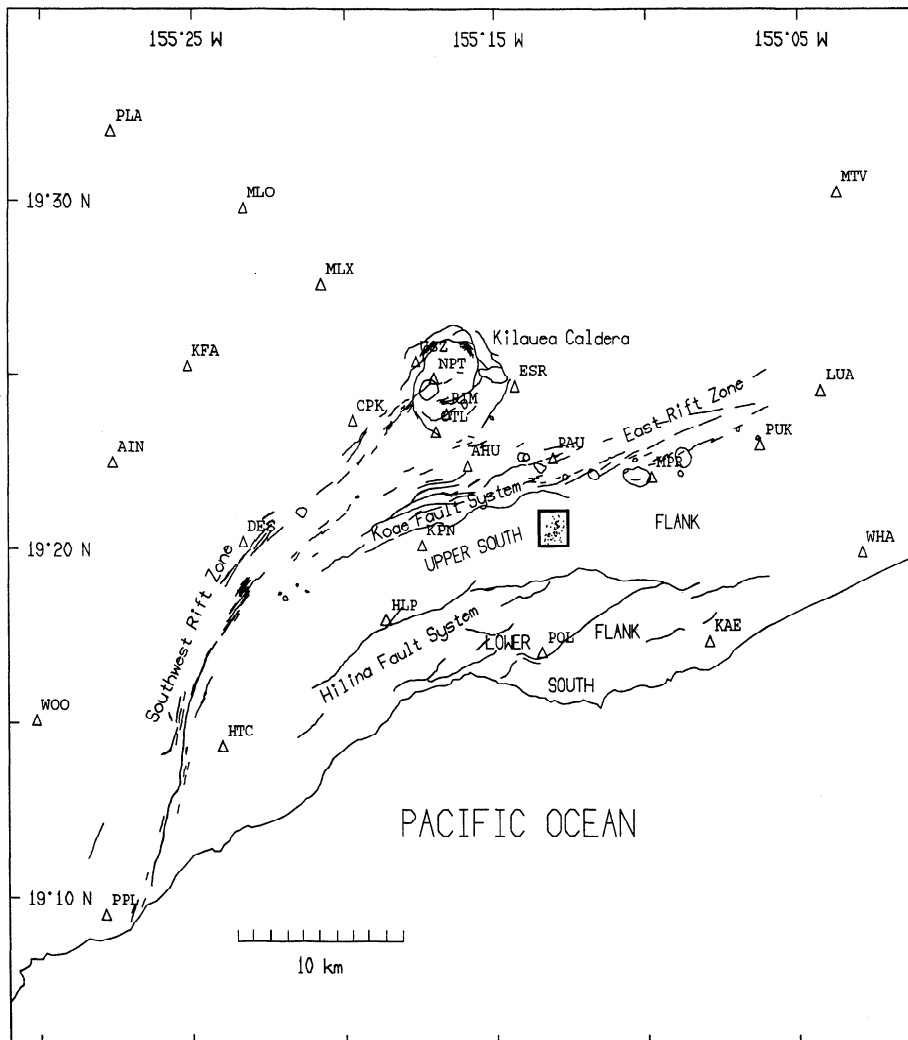
Figure 1a. Map of Kilauea volcano, Hawaii, showing the main geological features of the volcano (lines indicate the coast, rifts, and faults), the epicenters of the microearthquakes (dots) and the HVO seismic stations (open triangles) used in this study. The bold open square shows the limits of the map of the relative positions of the relocated events (Figure 1b).
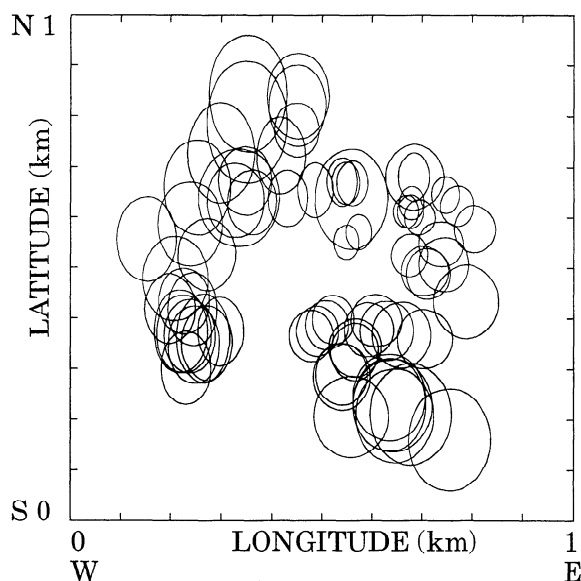
Figure 1b. Map of the relative positions of the events used in this study with their 90% confidence ellipses.
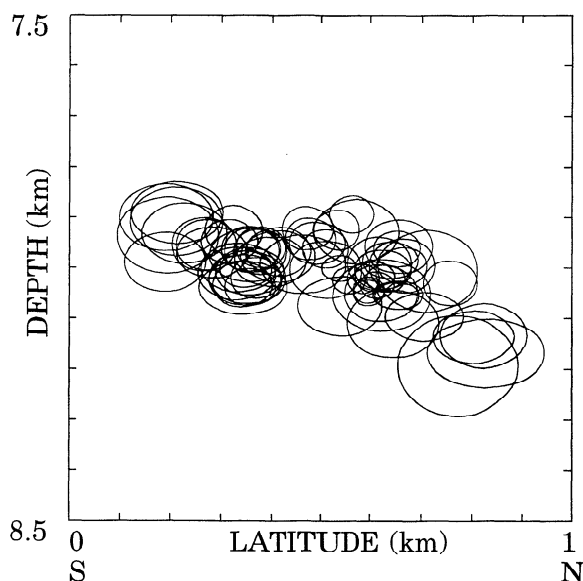
Figure 1c. North-south vertical cross section of the relative relocations of the multiplet events with their 90% confidence ellipses.

visible in the south flank (Figure 1a). The seismic events we used in this study are not volcanic microearthquakes of the caldera or the rift zones, but tectonic microearthquakes directly related to the southward displacement of the south flank of Kilauea volcano on its near-horizontal basal slip plane [*Got et al.*, 1994]. We kept for this study the events having the lowest vertical uncertainties; the average uncertainty for the relative relocations is about 50 m horizontally and vertically. The hypocenters are located along a nearly horizontal plane (Figures 1b and 1c), at an average depth of 8 km corresponding to that of the basal slip plane [*Got et al.*, 1994]. The event local magnitude is small, ranging from 1.0 to 2.5, but each event was recorded by at least 12 HVO stations. For this study, we use 9 stations located at hypocentral distances ranging from 10 to 20 km, with an available recording duration of about 4 times the S wave travel time. Energy and coherency between multiplet events remain sufficiently high in the coda (Figure 2) to compute travel time delays in the coda using the cross-spectral method. This set of similar events thus provides an array of microearthquakes with a density and distribution (71 epicenters on a 1 km^2 surface (Figures 1b and 1c)) well suited for near-source coda wave field studies.

However, there are three sources of error, or noise, associated with this data set, which could possibly degrade the quality of our results. First, S wave velocity may have undergone strong temporal variations during the period spanned by the data (1979-1983), when numerous intrusions and some eruptions occurred. These changes could be responsible for time delays between multiplet records and hence reduce the accuracy in slowness measurements. In order to minimize these effects, we selected 71 events from the initial 250-event multiplet, composed of events occurring during 27 short periods (less than 1 week). Assuming that the propagating medium experienced only limited velocity changes during these 27 time intervals where no apparent volcanic activity has been reported, we consider the 71 event cluster as being constituted of 27 subclusters, or subarrays, forming 83 event pairs in which the ray paths are identical for each event. The question of how medium velocity changes between subarrays can affect the ray path will be discussed as an introduction to the slowness vector computation.

Second, the acquisition process operated by HVO until 1983 used frequency-modulated signals recorded on 1 inch magnetic tapes, then demodulated and converted to 100-Hz, 10-bit digital data. Although the dynamical range is not large (50 to 60 dB), the data are convenient because they consist in low-noise, well-recorded, small-magnitude local micro-earthquakes whose amplitudes are not clipped by the recording system. However, tape speed could vary slowly during the process, causing time-dependent instrumental delays. Fortunately, all station signals used in this study were recorded on the same tape, enabling a simple correction that we detail later.

Third, the multiplets are composed of small-magnitude events which provide only short duration seismograms (20-25 s), forcing us to use stations located at short hypocentral distances (about 10 km) to study the late coda. This limitation restricts our study to short hypocentral distances. However, small-magnitude microearthquakes have been extensively used to infer coda-Q temporal variations [e.g., *Peng et al.*, 1987; *Huang and Wyss*, 1988; *Jin and Aki*, 1989; *Beroza et al.*, 1995], or S-wave velocity temporal variations from time delay measurements in seismic doublets [*Poupinet et al.*, 1984; *Ratdomopurbo and Poupinet*, 1995] and are generally taken as representative of crustal coda wave generation process.

Method

Time Delay Computation

Time delays for each pair of events recorded at each station are computed along the seismogram with a moving window technique [*Poupinet et al.*, 1984; *Fréchet*, 1985] using the classical cross-spectral method [*Jenkins and Watts*, 1968]. The time delay is computed for each window by a weighted linear fit of the cross-spectrum phase, the weight being a function of the coherency, which is inversely proportional to the phase error [*Poupinet et al.*, 1984; *Fréchet*, 1985]. The first window is centered on the theoretical P arrival time, calculated as the sum of the origin time for each event and the travel time from the

DOUBLET   800050215B4 - 800071131N4   STATION AHU
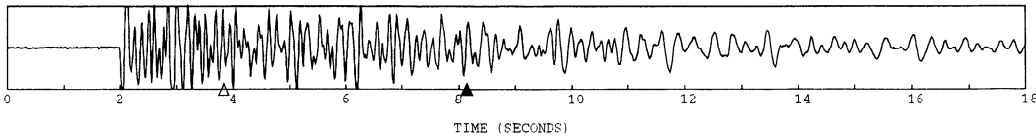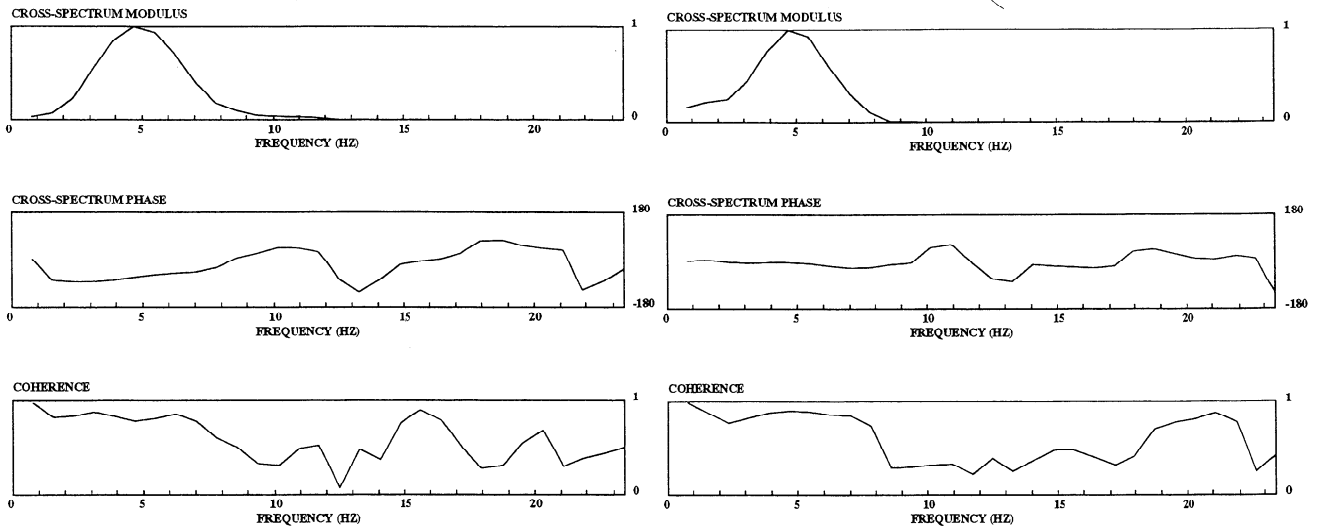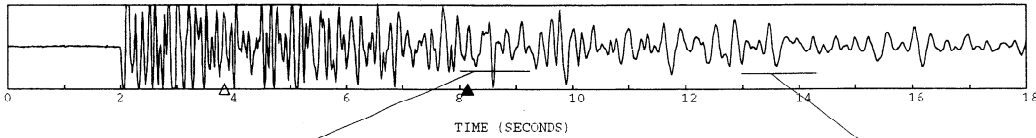
Figure 2. Seismograms, velocity cross-spectrum (modulus and phase) and coherence as a function of frequency, for a sample of doublets recorded at station AHU.

multiplet center to the receiver. We used 1.28 s-wide moving windows tapered with a Hanning cosine function. The window was moved 0.30 s at each step, so that two consecutive windows overlapped by about 75%.

Computation of the Slowness Vector Along the Seismogram

As was mentioned before, changes in the propagating medium could occur during the long time interval separating the first and the last event in the multiplet and could induce time delays and a loss of similarity between their waveforms. This would affect the accuracy of all methods based on waveform stacking such as beam forming, or F-K transforms [e.g., *Spudich and Bostwick*, 1987, equation (10)] when using the whole data set (71 events). On the other hand, stacking only inside subarrays would reduce their efficiency. We rather prefer to estimate slowness vectors using travel time delays expected to be due, as far as possible, to source location offsets. We therefore restrict these measurements to events belonging to the same subarray. We can expect to obtain more accurate slowness estimates by proceeding this way, that is, by comparing only waveforms affected mainly by geometrical time delays (that is, travel time delays produced only by different source locations). What happens however, if the medium velocity changes between the period of activity of two subarrays? Let us assume that these velocity perturbations occur far from the source area, which is not located in the vicinity of the caldera and the related magmatic system, but in the south flank of Kilauea (Figure 1a). They will affect mainly the travel

times and the waveforms of a wavelet, but not the direction along which it has left the source. Thus the arrival time of this wavelet will change for each subarray, but the travel time delay due only to the different source locations will remained unchanged. Since the travel time delay is estimated using finite length windows, as long as the wavelet remains in the same window, it will not affect the travel time delay measurement.

The relative relocation of the sources of this multiplet [*Got et al.*, 1994; Figures 1b and 1c] shows that the events are confined in a volume whose dimensions are negligible relative to the source-station distance. Therefore inside a subarray, the travel time difference is assumed to be due only to different source location. This hypothesis will be checked further by examining the azimuthal distribution of the travel time delay. Let $\Delta t_{ij}^{\,k}$ (t) be the difference in arrival time at station k between events i and j, for the time window centered at t. We therefore have

$$\Delta t_{ij}^{\,k}(t) = \Delta t_{orij} + \mathbf{r}_{ij}.\mathbf{s}^k(t) = \Delta t_{orij} + x_{ij}s_x^{\,k}(t) + y_{ij}s_y^{\,k}(t) + z_{ij}s_z^{\,k}(t) \qquad (1)$$

where $\mathbf{s}^k(t) = (s_x^{\,k}(t),\ s_y^{\,k}(t),\ s_z^{\,k}(t))^{\mathrm{T}}$ is the slowness vector for the station k and the time t, $\mathbf{r}_{ij} = (x_{ij},\ y_{ij},\ z_{ij})^{\mathrm{T}}$ is the source relative position vector for the (i,j) pair and Δt_{orij} is the origin time difference for the same pair. Recall here that the first window is centered on a theoretical arrival time, computed as the sum of the origin time of each event and a common travel time. Then the arrival time delay is computed, in each window, from the cross-spectral analysis of each pair of seismograms. This arrival time

delay would be exactly equal to the travel time delay if there were no error in the origin time. However, origin times are calculated with errors, so that we can finally write

$$\Delta T_{ij}^{\ k} = \Delta t_{ij}^{\ k} - \Delta t_{orij} = \delta t_{ij}^{\ k} - \delta t_{orij} \tag{2}$$

where $\delta t_{ij}^{\ k}$ is the arrival time difference computed from the cross-spectral analysis of the first window of the seismograms, and δt_{orij} is the error in origin times, common to all stations recording the pair (i,j). During the relative relocation process, r_{ij} and δt_{orij} are computed from

$$\mathbf{r}_{ij}.\mathbf{s}^k + \delta t_{orij} = \delta t_{ij}^{\ k} \tag{3}$$

$\mathbf{s}^k$ being determined by the direct ray path between the absolute location of the cluster center and the station k. Note that δt_{orij}, and therefore $\Delta T_{ij}^{\ k}(t)$ are known only after the relocation process has been completed. Thus, the slowness at any time $\mathbf{s}^k(t)$ can be computed from the travel-time delay $\Delta T_{ij}^{\ k}(t)$ as

$$\Delta T_{ij}^{\ k}(t) = \delta t_{ij}^{\ k}(t) - \delta t_{orij} = \mathbf{r}_{ij}.\mathbf{s}^k(t) \tag{4}$$

where $\delta t_{ij}^{\ k}(t)$ is measured, r_{ij} and δt_{orij} are given by the relocation process, and $\mathbf{s}^k(t)$ is unknown.

$\Delta T_{ij}^{\ k}(t)$ are estimated for event pairs (i,j) belonging to the same subarray. For a given station k we therefore have to solve a system of linear equations for each time window:

$$\mathbf{R}\mathbf{s}^k = \mathbf{d}^k \tag{5}$$

where the matrix $\mathbf{R}$ and vector $\mathbf{d}^k$ are built from r_{ij} and $\Delta T_{ij}^{\ k}$, respectively. This linear system is solved by the normal equation method:

$$\mathbf{R}^T\mathbf{C}_d^{-1}\mathbf{R}.\mathbf{s}^k = \mathbf{R}^T\mathbf{C}_d^{-1}\mathbf{d}^k \tag{6}$$

from which

$$\mathbf{s}^k = \left(\mathbf{R}^T\mathbf{C}_d^{-1}\mathbf{R}\right)^{-1}\mathbf{R}^T\mathbf{C}_d^{-1}\mathbf{d}^k \tag{7}$$

where $\mathbf{C}_d$ is the data covariance matrix, computed from the time delay error. The vector $\mathbf{d}^k$ is determined by a moving window technique, which allows the computation of $\mathbf{s}^k$ along the whole seismogram.

Errors in Travel Time Delay and Slowness Estimates

On the basis of equation (2), there are two sources of error when estimating $\Delta T_{ij}^{\ k}(t)$: the origin time error and the instrumental delay introduced by tape speed variations. The estimate of the origin time error is a result of the relative relocation process. It is the same for all stations and does not depend on the time t. Instrumental delay, on the contrary, varies with time and is not a result of the relocation process. Poupinet et al. [1984] and Fréchet [1985] inferred instrumental delays induced by tape speed variations from the cross-spectral analysis of the reference sinusoids recorded with the seismic signal on each magnetic tape. Unfortunately, these sinusoids were not digitized by HVO and therefore were not available for this study. However, all records used in this study were stored on a single tape, so that the instrumental delays are identical for all stations. This last feature allows us to compute the correction $\delta T_{ij}(t)$ due to

instrumental delays in a simple way. First, the origin time error δt_{orij} actually contains the instrumental delay due to tape speed variations in the first time window. Second, the variation of $\delta T_{ij}(t)$ between two consecutive windows is supposed to be small because of the nature of the instrumental process (tape speed variation) and the 75% overlap in consecutive windows. The moderate change in $\delta T_{ij}(t)$ and its equality for all stations allows us to compute, in each window for every station k, the current value of the slowness vector $\mathbf{s}^k$, using the current time delay and the correction $\delta T_{ij}(t)$ computed at the earlier position of the window. In the next step, $\delta^2 T_{ij}(t)$ (variation of $\delta T_{ij}(t)$), is computed for the current window as the average of the weighted residuals calculated for each pair (i,j) over the whole set of nine stations. Finally $\delta T_{ij}(t)$ is updated for the current window, and $\mathbf{s}^k$ is calculated using this final value of $\delta T_{ij}(t)$. Hereinafter, the travel time delay corrected from $\delta T_{ij}(t)$ will be denoted $\Delta T_{ij}^{\ k}(t)$ and referred to simply as travel time delay

$$\Delta T_{ij}^{\ k}(t) = \delta t_{ij}^{\ k}(t) - \delta t_{orij} - \delta T_{ij}(t) \tag{8}$$

Errors in slowness estimates are directly due to errors in travel time delay $\Delta T_{ij}^{\ k}(t)$ and in relative locations. We assume that there is no bias in the relative locations r_{ij}, or in $\Delta T_{ij}^{\ k}(t)$ after correction for $\delta T_{ij}(t)$. To consider error in the relative relocations (the model) and not only in $\Delta T_{ij}^{\ k}(t)$ (the data), we estimate the uncertainty in the determination of $\mathbf{s}^k$ from a Monte Carlo simulation using random perturbations of $\delta t_{ij}^{\ k}(t)$ and r_{ij}.

Results

Time Delay Computation

Time delays have been calculated for windows along the complete seismograms, using every event pair in subarrays and for nine stations. Figure 3 presents selected event pairs recorded at several stations. This sample of the results shows that travel time delay clearly varies with time in the coda for many stations (e.g., AHU, OTL, RIM, ESR). The amplitude of the $\Delta T_{ij}^{\ k}(t)$ variations can reach 100 ms for some stations between the first arrivals and the late coda (Figure 3). Travel time delay $\Delta T_{ij}^{\ k}(t)$ can increase or decrease depending on the event pair and the station used. $\Delta T_{ij}^{\ k}(t)$ can be positive in the first arrivals and negative in the coda, or vice versa. These changes of sign in $\Delta T_{ij}^{\ k}(t)$ along the seismogram cannot be explained by S wave velocity temporal variations. To understand the features of these variations, and to determine if their cause is spatial or temporal, we represent the travel time delay as a function of the azimuth of the relocation vector r_{ij} (Figure 4).

Recalling that the geometrical travel time delay $\Delta T_{ij}^{\ k}(t)$ is expressed as the dot product of the slowness vector $\mathbf{s}^k$ and the relative location vector r_{ij} (equation (4)), let Az^k and Ain^k be the azimuth and take-off angles of the slowness vector $\mathbf{s}^k$. Az_{ij} and Dip_{ij} are the azimuth and the dip angles, respectively, of the relative location vector $r_{ij} = (x_{ij}, y_{ij}, z_{ij})^T$, r_{ij} its modulus, and V the velocity in the vicinity of the hypocenters. We find from (4), for each time window:

$$\frac{V\Delta T_{ij}^k - z_{ij}\cos Ain^k}{r_{ij}\sin Ain^k \sin Dip_{ij}} = \cos(Az^k - Az_{ij}) \tag{9}$$
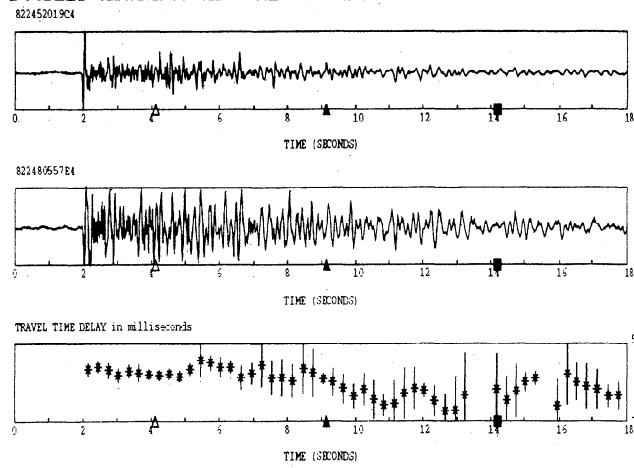
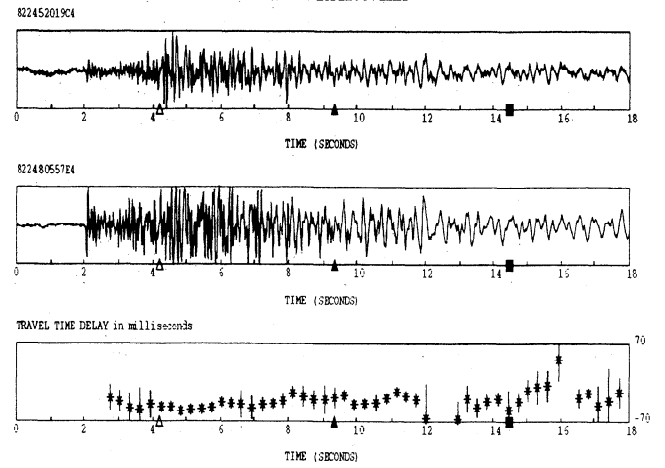DOUBLET 800050215B4 - 800071131N4   STATION RIM
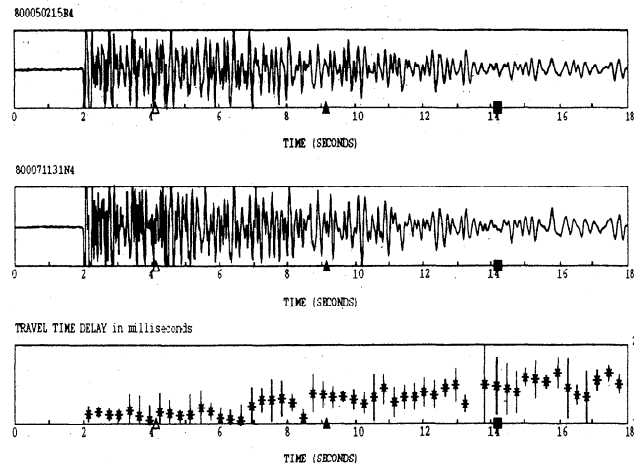
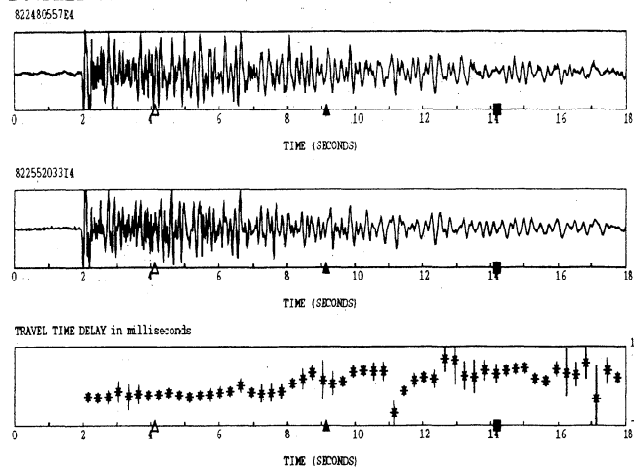DOUBLET 800050215B4 - 800071131N4   STATION HLP
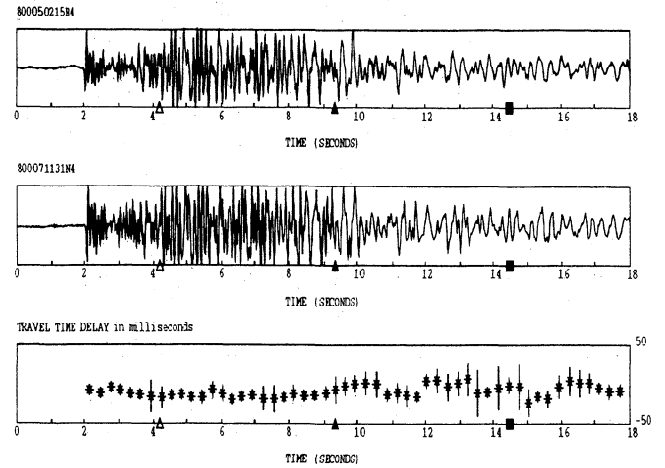
DOUBLET 822452019C4 - 822480557E4   STATION RIM

DOUBLET 822452019C4 - 822480557E4   STATION HLP

DOUBLET 822480557E4 - 82255203314   STATION RIM
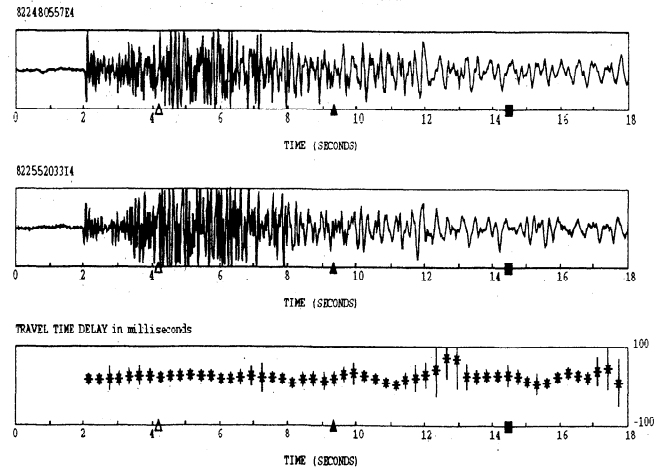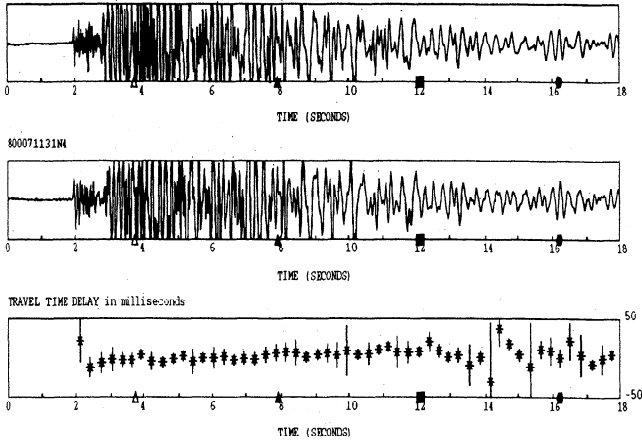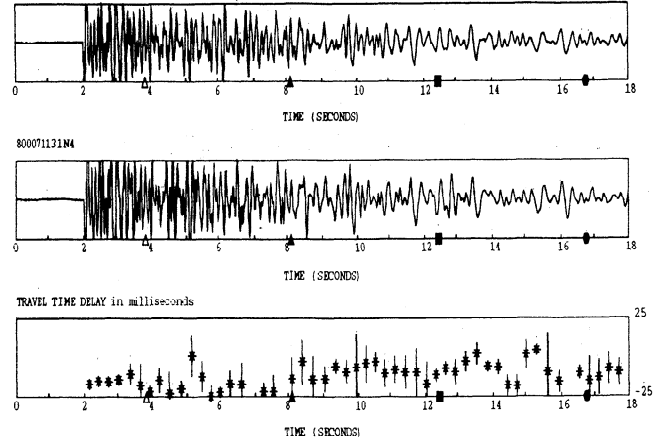
DOUBLET 822480557E4 - 82255203314   STATION HLP

Figure 3. Seismograms and travel time delay (with confidence intervals) as a function of time for a sample of doublets recorded at six seismic stations. Open triangles, solid triangles, squares, and ovals indicate t_S, $2t_S$, $3t_S$ and $4t_S$, respectively.

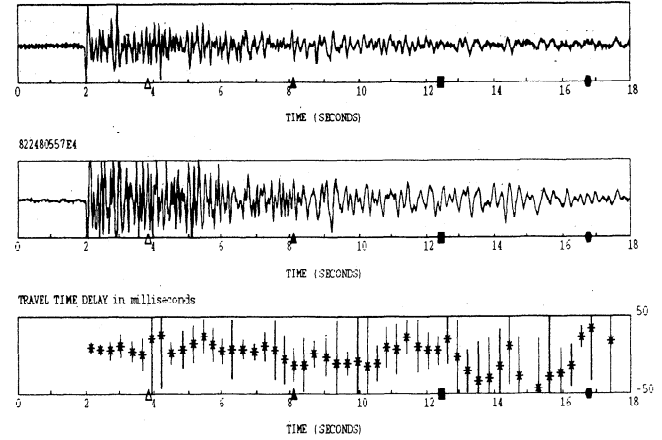DOUBLET 800050215B4 - 800071131N4   STATION MPR

DOUBLET 800050215B4 - 800071131N4   STATION AHU

DOUBLET 822452019C4 - 822480557E4   STATION MPR
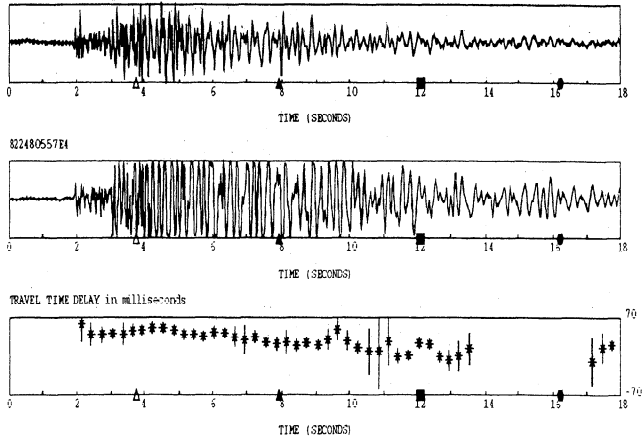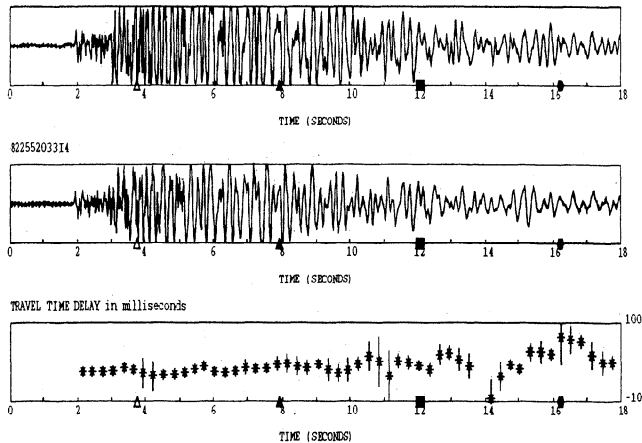
DOUBLET 822452019C4 - 822480557E4   STATION AHU

DOUBLET 822480557E4 - 82255203314   STATION MPR

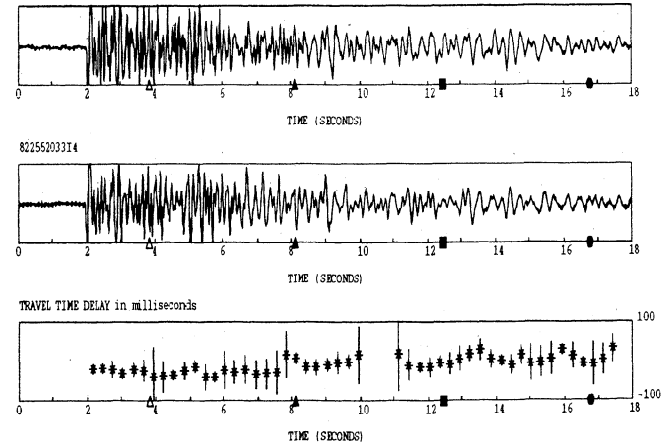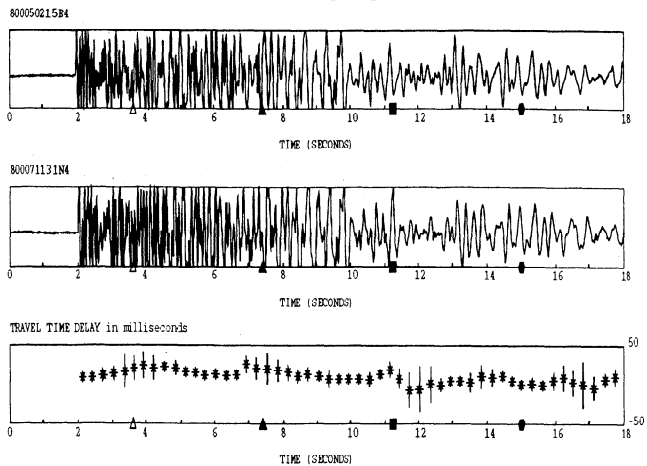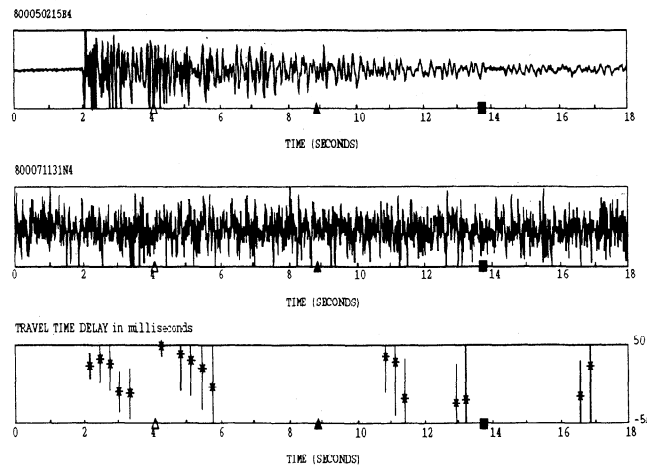DOUBLET 822480557E4 - 82255203314   STATION AHU
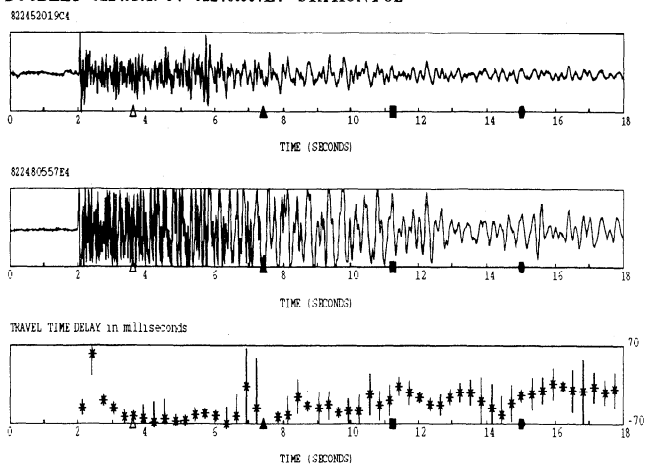
Figure 3. (continued)

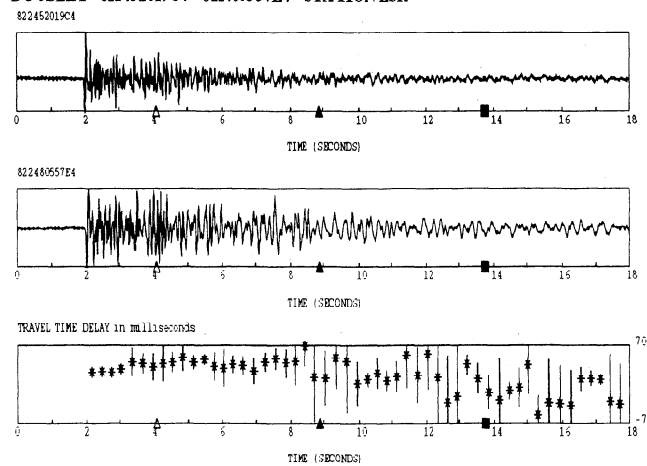DOUBLET 800050215B4 - 800071131N4   STATION POL

DOUBLET 800050215B4 - 800071131N4   STATION ESR
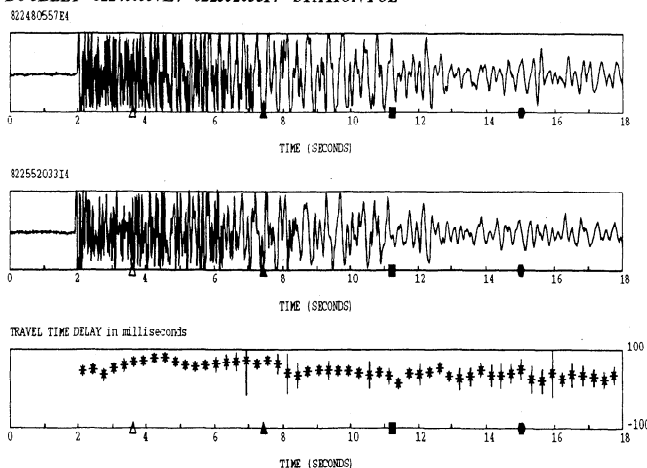
DOUBLET 822452019C4 - 822480557E4   STATION POL

DOUBLET 822452019C4 - 822480557E4   STATION ESR

DOUBLET 822480557E4 - 822552033I4   STATION POL

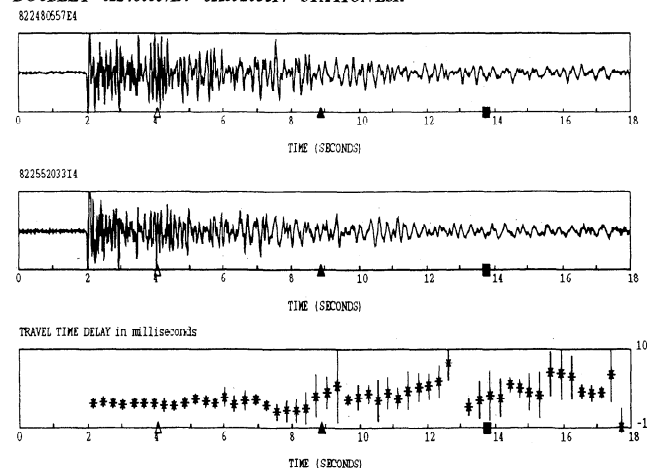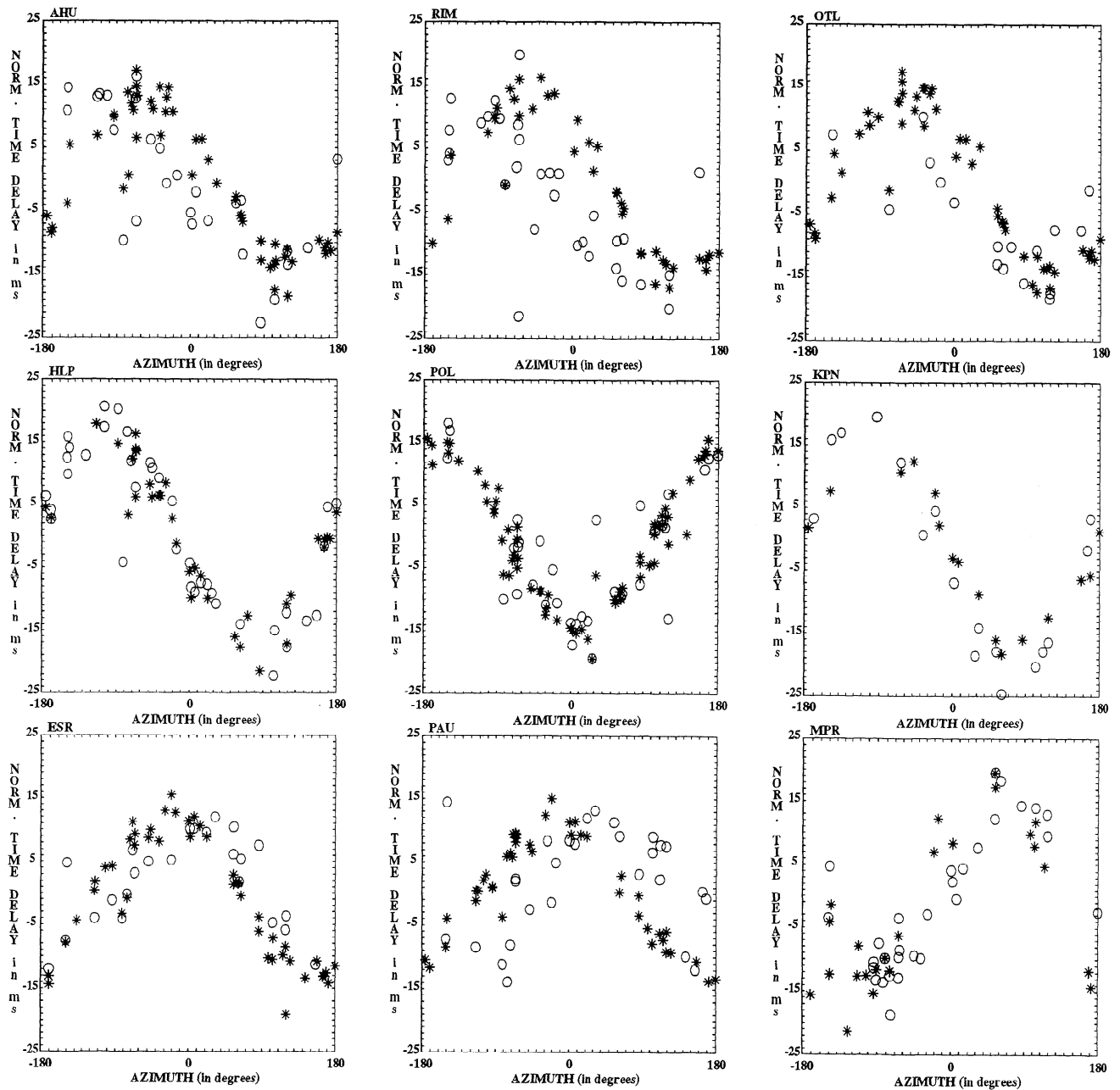DOUBLET 822480557E4 - 822552033I4   STATION ESR

Figure 3. (continued)

Figure 4. Normalized travel time delay τ computed in the first arrivals (stars) and in the late coda at about $3t_S$ (circles) as a function of the azimuth of $\mathbf{r}_{ij}$, for each station. Notice that τ corresponds to a normalized interevent distance and cannot be directly compared to the actual travel time delay.

Let τ, the left-hand side of equation (9) times 10 ms, be a "normalized travel time delay". Provided that $\Delta T_{ij}{}^k$ is actually of geometrical origin, the representation of τ as a function of Az_{ij} in the first arrivals should be a sinusoid with a maximum reached for $Az_{ij} = Az^k$, the s^k slowness vector azimuth. In Figure 4 we plot τ as a function of Az_{ij} for each station k, with $\Delta T_{ij}{}^k$ computed for the P first-arrival window (stars) and for a late coda window (circles). The sampling of the azimuth domain by the event pairs and the accuracy of the travel time delay measurements allow us to recognize that, for both windows, τ is varying as a sinusoid. Plots of τ corresponding to the P first arrival show a maximum for a slowness vector azimuth corresponding to the direct ray, and

τ plots for the coda window also show a sinusoid strikingly similar to that of the first arrival. The τ plots for first arrival and coda windows are almost superposed for the station HLP (see Figure 4), which shows no steady variations of the time delay along the seismogram (Figure 3). Stations AHU, OTL, RIM and ESR show strong variations of $\Delta T_{ij}{}^k$ along the seismograms (Figure 3), and τ plots for coda windows, similar but clearly shifted relative to first arrival windows (Figure 4). Each value of τ (star or circle) corresponds to a given event pair spanning a given period of time between 1979 and 1983 (each period being shorter than 1 week). Random velocity variations during these periods would disturb randomly the azimuthal pattern predicted

for τ by (9). The good fit to a sinusoid and the striking similarity of τ azimuthal patterns between the first arrivals and the coda observed in Figure 4 show that the part of the time delay due to velocity variations is small. This allows us to discard temporal variations in S wave (or P wave) velocity during the periods spanned by each doublet as an explanation for the travel time delay variations exhibited by Figure 3 and therefore supports the hypothesis founding our computation (equation (1)) of the slowness vector along the seismogram. The shift of the coda τ plots for many stations can merely be interpreted as a rotation of the coda slowness vector. Consequently, in the next section, we consider the time delay as due purely to the difference in event locations, and its time variations as due to slowness vector rotations. The slowness vector is now inverted using equation (7) for windows along the whole seismogram, in order to study the change of its direction with time; the weak effect of velocity variations on time delays will be considered as a noise on data during the inversion process.

Slowness Vector Computation

The slowness vector $\mathbf{s}^k$ is computed for each station k, using the set of 83 event pairs (that is, 83 equations for each station) from travel time t_p to $4t_s$. Beyond this lapse time the coherency is generally too low to allow accurate computations of the time delay and the slowness vector. To consider errors in the relative relocations and in the data, we perform a Monte Carlo simulation using 1000 random perturbations of ΔT_{ij}^k and $\mathbf{r}_{ij}$ that yields an estimate of the uncertainties in the determination of $\mathbf{s}$. Standard deviation is 10 ms for the time delay and 50 m for each coordinate of $\mathbf{r}_{ij}$. Azimuths and takeoff angles of $\mathbf{s}$ are determined in the coda with an average uncertainty of about 5° and 10° to 15°, respectively. It is clear from equation (4) that the relatively poor angular resolution we obtained for the takeoff angle is due to the poor vertical range of our relative relocation set. Conversely, azimuth angular resolution is better owing to the good azimuthal coverage of $\mathbf{r}$.

From the Monte Carlo computation of $\mathbf{s}$ we get 1000 estimates of $\mathbf{s}$ for each time window. Rather than represent $\mathbf{s}$ as a function of time, we decided to represent the time (elapsed from the first P arrival) corresponding to each wavelet for which $\mathbf{s}$ has been computed, as a function of the direction of $\mathbf{s}$. Since the energy constituting coda waves is completely radiated upward, results of the slowness vector computation are plotted using a stereographic projection of the upper focal hemisphere (Figure 5). The time represented in a given direction of the upper focal hemisphere is the average of the centers of the time windows having slowness vectors whose directions belong to the 0.5° azimuth, 0.5° takeoff angle, spatial window centered on that given direction. The stereographic projections show azimuthal patterns coherent with those observed in time delay measurements (Figure 4). The slowness for stations HLP, POL, and KPN shows that the coda waves are strikingly emitted in directions very close to that of the direct ray. In contrast, for the other stations, coda waves are emitted in various directions. However, these directions do not appear to have a random distribution. On the one hand, for stations RIM, OTL, and AHU, wavelets in the late coda are emitted westward and southwestward, whereas the direct ray is emitted northwestward. On the other hand, stations ESR, PAU and MPR exhibit eastward clockwise rotations of the slowness vector with time. The entire set of stations does not provide any example of crustal isotropic scattering. Figure 6 is a summary plot, showing time delay variations, event relative positions, and slowness vectors for the sample of doublets shown in Figure 3 for

station RIM. For the doublet 800050215B4 - 800071131N4, for instance, the relative position vector denoted $\mathbf{r}_{12}$ has an azimuth of approximately N320°. Since the first arrivals leave the hypocenters with the same azimuth of N320°, the travel time delay in the first arrivals is negative, with a maximum absolute value. The counterclockwise rotation of the slowness vector corresponds to a decrease of this travel time delay absolute value. It becomes zero between $3t_s$ and $4t_s$ with a corresponding slowness vector azimuth of about N230° (that is, at this time, $\mathbf{s}^{RIM}$ is normal to $\mathbf{r}_{12}$). For the doublet 822480557E4 - 822552033I4 the relative position vector, denoted $\mathbf{r}_{34}$, has an azimuth of approximately N10°. First arrivals leave the hypocenters with an azimuth of N320°. Therefore the difference in the azimuth of $\mathbf{s}^{RIM}$ and $\mathbf{r}_{34}$ is about 50°. Travel time delay is negative in the first arrivals and becomes positive at approximately $2t_s$, corresponding to a slowness vector azimuth of N280° (Figure 6). The travel-time delay continues to increase until 3 to $4t_s$, which corresponds to a slowness vector azimuth of N230°. This coherent set of observations (Figure 6) suggests that purely geometric effects can explain time delay variation patterns in the coda that could erroneously be attributed to S wave velocity variations. These geometric effects could be observable in coda travel time delays in any situation where nonisotropic propagation of coda waves exists. Such effect would become stronger as the distance r between doublet events increases.

Discussion and Conclusion

Time delays computed along the seismograms of microearthquake doublets have been generally used to infer S wave velocity temporal variations [Poupinet et al., 1984; Ratdomopurbo and Poupinet, 1995]. However, our results show that travel time delay can vary along the seismogram even for a pair of events between which no temporal variation is expected (Figure 3). Despite the variation of the travel time delay along the seismogram, the azimuthal pattern exhibited by the (normalized) travel time delay τ computed for various event pairs in the first arrivals is preserved in the coda. Figure 4 shows that the only consequence of the variation of the travel time delay along the seismogram is the shift of the azimuthal pattern of τ. Figure 4 and the computation of the slowness vector show that for each window, the azimuthal distribution of the time delays calculated for the whole set of the 83 event pairs used can be explained by a unique direction of the slowness vector. Therefore time delay variations along the coda could have a spatial origin. For instance, events separated by a distance of about 500 m can have a time delay variation between the first arrival and the coda of up to 0.1 s, which is greater than most time delay variations measured until now using doublets and interpreted as temporal S wave velocity changes [Poupinet et al., 1984; Ratdomopurbo and Poupinet, 1995]. Therefore our results suggest that S wave velocity variation estimations should be restricted to doublets with extremely close and highly accurate locations. In addition, interpretation of time delay variations in the early and late coda as S wave velocity variations involving a large volume of the upper crust has to be undertaken with extreme caution. Indeed, local surficial changes could induce similar variations in the time delays in the coda if this latter part of the seismogram was generated by multiple scattering, reverberation or surface wave conversion in the surface low-velocity layers close to the station.

Wavelets constituting the coda after $2t_s$ have been often modeled as single S waves backscattered by a random
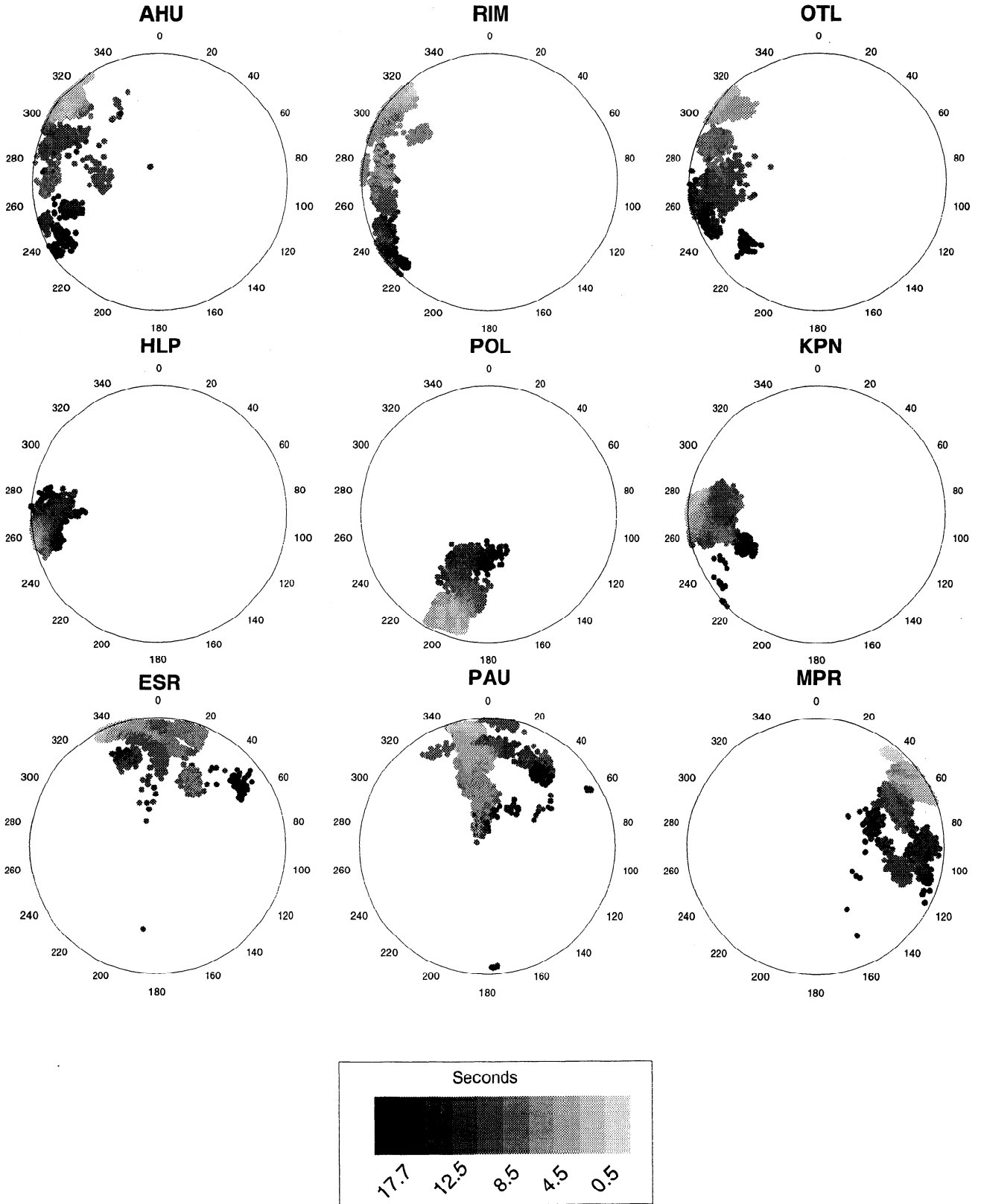
Figure 5. Time (elapsed from the P first arrival time) for the arrival of each wavelet as a function of the direction of its slowness vector s, represented by mean of a stereographic projection on the upper focal hemisphere. Slowness vector s is computed from the set of 83 doublets described in the text (see text for details). Average uncertainty in each s direction is about $5°$ and $10°$ to $15°$ for the azimuth and the takeoff angle, respectively. The lower grey level represents the early body waves (P first arrivals), and the higher grey levels represent the later parts of the seismogram. Time is computed for each degree of azimuth and takeoff angle as the average time over a narrow $0.5°$ azimuth, $0.5°$ takeoff angle, spatial window centered on that direction.
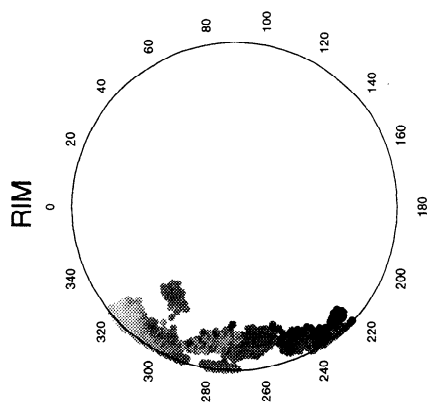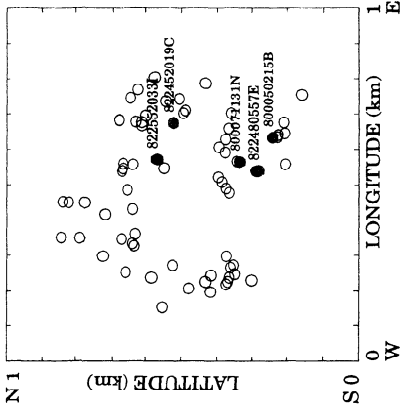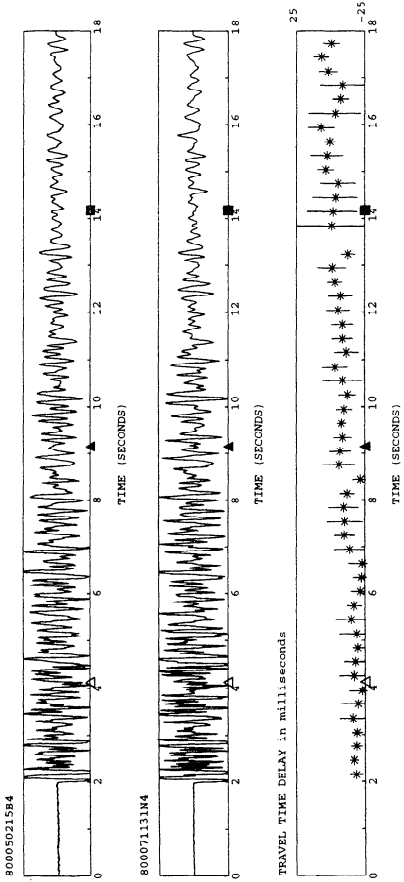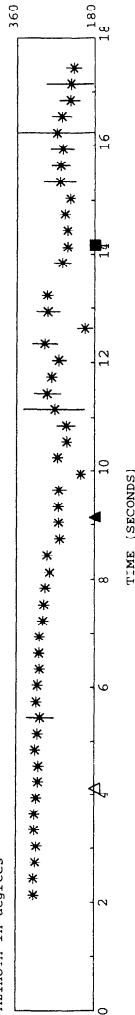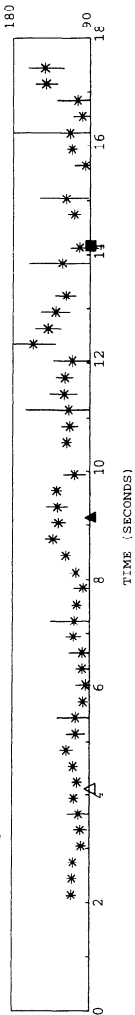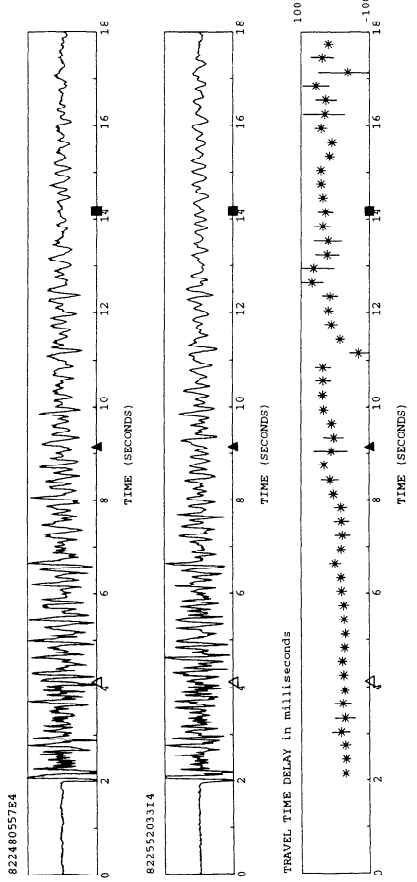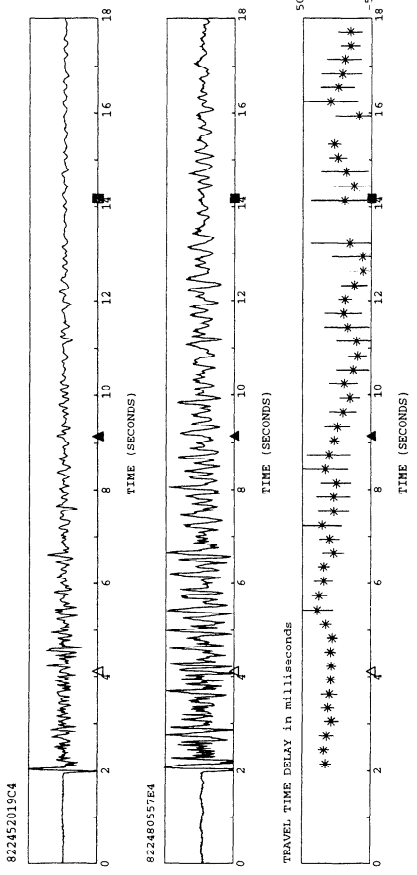
distribution of scatterers at depth [Aki and Chouet, 1975]. In such a model, late coda wavelets sample an ellipsoidal volume whose foci are taken as the source and the station. The dimensions of the sampled ellipsoidal volume of crust increase with the arrival time of the wavelets along the coda. Slowness vectors corresponding to such backscattered coda wavelets should therefore have random directions.

However, none of the patterns shown by the slowness vectors we have computed (Figure 5) can be interpreted as being random ones. Stations HLP, POL, and KPN show a distribution of slowness vectors strongly concentrated around the direct path, even for lapse times much later than twice the shear wave travel time. Such a distribution is very similar to that obtained from slowness power spectrum analysis by Spudich and Bostwick [1987], and Scherbaum et al. [1991] in the early coda. They interpreted these coda waves which left the source in directions close to the direct path as due to the multiple scattering of shear waves in the low velocity surface layers near the station. Alternatively, these upgoing coda waves can be S waves converted into surface waves in the surface layers [Levander and Hill, 1985; Liu and Heaton, 1984; Phillips and Aki, 1986]. Our results show that these phenomena can dominate the coda seismogram even for lapse times much later than $2t_S$. Stations HLP and POL are located in areas where topography is sharp (station HLP is situated just north of the Hilina fault scarps; POL is located near cracks, close to Holei Pali), low-velocity surface layers are present, and Q is relatively low at depth.

The other seismic stations that we used show broader azimuthal distributions of slowness vectors. The slowness vectors are not concentrated in the direction of the direct path; rather, their azimuth gradually rotates with time, whereas their takeoff angle remains pointing upward (Figure 5). This pattern is not likely from scattering of waves by randomly distributed heterogeneities in a homogeneous medium. It is striking that although the computations are independent for each station, the three neighboring stations RIM, OTL, and AHU exhibit very similar azimuthal distributions of slowness vectors. Later arrivals in the coda recorded at sites RIM, OTL, and AHU leave the source upward with the same southwestward direction. Furthermore, the strong nonisotropic character of the slowness vector's azimuthal distribution and the time duration of the phenomenon indicate that it could be caused by scattering or lateral reflection from one of the major geological discontinuities that reaches the surface in the south flank of Kilauea volcano (e.g., the Hilina fault scarps). However, the closeness of the three stations RIM, OTL, and AHU makes the accurate determination of scatterer locations impossible.

Results from all the stations show that the wave propagation remains strongly nonisotropic much later than twice the S wave travel time, that is, surficial multiple forward scattering or reverberation locally dominates the wave energy even in the "late" coda. Results from Hoshiba [1995] have already indicated that nonisotropic scattering can predominate in the early coda. Xie et al. [1996] found no significant difference in the coda wave slowness power spectrum at lapse times around $2t_S$. It should be

stressed, however, that although we do not provide evidence of deep scattering, our results do not mean that scattering does not occur deeper in Kilauea volcano. Our results only indicate that in this highly perturbed environment, where topography can be sharp and velocity low in the surface layers, multiple scattering, reverberation or surface wave conversion near the surface ("local scattering") can predominate over deep crustal scattering for lapse times far greater than $2t_S$. Consequently, the late coda should be defined as the part of the coda for which deep crustal scattering predominates over local surface scattering, without any reference to a fixed lapse time for its beginning. This conclusion is supported by results from Mayeda et al. [1991] and Koyanagi et al. [1992], who observed that in highly perturbed tectonic or volcanic environments showing unconsolidated quaternary deposits, (such as Long Valley caldera or Kilauea volcano), coda decay becomes common to the stations only after a lapse time much greater than $2t_S$. Such a search for a decay independent of the azimuth of the events used and common to a significant set of stations, comprising hardrock sites, seems to be a better practical approach to find the beginning of the late coda than the $2t_S$ rule of thumb. However, our study shows that in some environments (and typically on volcanoes), small-magnitude seismic events can lack this so-defined late coda and are therefore unsuitable for Q-coda computations using the single backscattering assumption. In addition, the interpretation of S wave velocity or attenuation variations computed from small-magnitude microearthquake doublets needs to take the actual coda wave propagation into account.

References

Aki, K., and B. Chouet, Origin of coda waves: Source, attenuation and scattering effects, J. Geophys. Res., 80, 3322-3342, 1975.

Al-Shukri, H.J., G.L. Pavlis, and F.L. III Vernon, Site effects observations from broadband arrays, Bull. Seismol. Soc. Am., 85, 1758-1769, 1995.

Beroza, G.C., T.A. Cole, and W.L. Ellsworth, Stability of coda wave attenuation during the Loma Prieta, California, earthquake sequence, J. Geophys. Res., 100, 3977-3987, 1995.

Dainty, A.M., and M.N.Toksöz, Array analysis of seismic scattering, Bull. Seismol. Soc. Am., 80, 2242-2260, 1990.

Fréchet, J., Sismogenèse et doublets sismiques, thèse d'Etat, Univ. Sci. Technol. Méd., Grenoble, France, 1985.

Got, J.-L., J. Fréchet, and F.W. Klein, Deep fault plane inferred from multiplet relative relocation in the south flank of Kilauea Volcano, Hawaii, J. Geophys. Res., 99, 15,375-15,386, 1994.

Herraiz, M., and A.F. Espinosa, Coda waves: A review, Pure Appl. Geophys., 125, 499-578, 1987.

Hoshiba, M., Estimation of nonisotropic scattering in western Japan using coda wave envelopes: Application of a multiple nonisotropic scattering model, J. Geophys. Res., 100, 645-657, 1995.

Figure 6. (opposite) Summary figure showing travel time delays computed for a sample of doublets, relative locations of the multiplet (relative locations of the sample of events are indicated by solid circles), azimuth and takeoff angle of s as a function of time, and slowness vectors s for station RIM. Slowness vector s is computed from the set of 83 doublets described in the text (see text for details). Refer to Figure 3 for the legend of the plot of the traveltime delay as a function of time, and to Figure 5 for the legend of the stereographic plot of the slowness vectors.

Huang, Z.X., and M. Wyss, Coda Q before the 1983 Hawaii (M_s = 6.6) earthquake, *Bull. Seismol. Soc. Am.*, *78*, 1279-1296, 1988.

James, D.E., T.J. Clarke, and R.P. Meyer, A study of seismic reflection imaging using microearthquake sources, *Tectonophysics*, *140*, 65-79, 1987.

Jenkins, G.M., and D.G. Watts, *Spectral Analysis and Its Applications*, Holden-Day, Merrifield, Va., 1968.

Jin, A., and K. Aki, Spatial and temporal correlation between coda Q^{-1} and its physical mechanism, *J. Geophys. Res.*, *94*, 14,041-14,059, 1989.

Koyanagi, S., K. Mayeda, and K. Aki, Frequency-dependent site amplification factors using the S-wave coda for the island of Hawaii, *Bull. Seismol. Soc. Am.*, *82*, 1151-1185, 1992.

Levander, A.R., and N.R. Hill, P-SV resonances in irregular low-velocity surface layers, *Bull. Seismol. Soc. Am.*, *75*, 847-864, 1985.

Liu, H.-L., and T. Heaton, Array analysis of the ground velocities and accelerations from the 1971 San Fernando, California, earthquake, *Bull. Seismol. Soc. Am.*, *74*, 1951-1968, 1984.

Mayeda, K., S. Koyanagi, and K. Aki, Site amplification from S-wave coda in the Long Valley caldera region, California, *Bull. Seismol. Soc. Am.*, *81*, 2194-2213, 1991.

Mayeda, K., S. Koyanagi, M. Hoshiba, K. Aki, and Y. Zeng, A comparative study of scattering, intrinsic, and coda Q^{-1} for Hawaii, Long Valley, and central California between 1.5 and 15.0 Hz, *J. Geophys. Res.*, *97*, 6643-6659, 1992.

Peng, J.Y., K. Aki, W.H.K. Lee, B. Chouet, P. Johnson, S. Marks, J.T. Newberry, A.S. Ryal, S.W. Stewart, and D.M. Tottingham, Temporal change in coda Q associated with 1984 Round Valley earthquake in California, *J. Geophys. Res.*, *92*, 3507-3536, 1987.

Phillips, W.S., and K. Aki, Site amplification of coda waves from local earthquakes in Central California, *Bull. Seismol. Soc. Am.*, *76*, 627-648, 1986.

Poupinet, G., W.L. Ellsworth, and J. Fréchet, Monitoring velocity variations in the crust using earthquake doublets: An application to the Calaveras fault, California, *J. Geophys. Res.*, *89*, 5719-5731, 1984.

Ratdomopurbo, A., and G. Poupinet, Monitoring a temporal change of seismic velocity in a volcano: application to the 1992 eruption of Mt. Merapi (Indonesia), *Geophys. Res. Lett.*, *22*, 775-778, 1995.

Rautian, T.G., and V.I. Khalturin, The use of the coda for the determination of the earthquake source spectrum, *Bull. Seismol. Soc. Am.*, *68*, 923-948, 1978.

Sato, H., Attenuation and envelope formation of three-component seismograms of small local earthquakes in randomly inhomogeneous lithosphere, *J. Geophys. Res.*, *89*, 1221-1241, 1984.

Sato, H., Study of seismogram envelopes based on scattering by random inhomogeneities in the lithosphere: A review, *Phys. Earth Planet. Inter.*, *67*, 4-19, 1991.

Scherbaum, F., D. Gillard, and N. Deichmann, Slowness power spectrum analysis of the coda composition of two microearthquake clusters in northern Switzerland, *Phys. Earth. Planet. Inter.*, *67*, 137-161, 1991.

Spudich, P., and T. Bostwick, Studies of the seismic coda using an earthquake cluster as a deeply buried seismograph array, *J. Geophys. Res.*, *92*, 10526-10546, 1987.

Spudich, P., and M. Iida, The seismic coda, site effects, and scattering in alluvial basins studied using aftershocks of the 1986 North Palm Springs, California, earthquake as source arrays, *Bull. Seismol. Soc. Am.*, *83*, 1721-1743, 1993.

Spudich, P., and D.P. Miller, Seismic site effects and the spatial interpolation of earthquake seismograms: Results using aftershocks of the 1986 North Palm Springs, California, earthquake, *Bull. Seismol. Soc. Am.*, *80*, 1504-1532, 1990.

Xie, J., L. Cong, B.J. Mitchell, and J.M. Chiu, Complexities in high-frequency seismic waveforms due to three-dimensional structure in the New Madrid seismic zone, *J. Geophys. Res.*, *101*, 5751-5778, 1996.

O. Coutant, Laboratoire de Géophysique Interne et Tectonophysique, CNRS, Université Joseph Fourier, 38041 Grenoble, France. (e-mail: coutant@lgit.observ-gr.fr)

J.-L. Got, Laboratoire d'Instrumentation Géophysique, Université de Savoie, 73376 Le Bourget-du-Lac, France. (e-mail: got@univ-savoie.fr)